Supporting Information for

Large Bandgap of Pressurized Trilayer Graphene

Feng Ke[1#],Yabin Chen[2#], Ketao Yin[3#], Jiejuan Yan[1,4], Hengzhong Zhang[1], Zhenxian Liu[5], John S. Tse[3], Junqiao Wu[2], Ho-Kwang Mao[1]*,and Bin Chen[1]*

[1]*Center for High Pressure Science and Technology Advanced Research, Shanghai 201203, China*

[2]*Department of Materials Science and Engineering, University of California, Berkeley, California 94720, USA*

[3]*Department of Physics and Engineering Physics, University of Saskatchewan, Saskatoon, Saskatchewan, S7N 5E2, Canada*

[4]*Advanced Light Source, Lawrence Berkeley National Laboratory, Berkeley, CA94720*

[5]*Institute of Materials Science, Department of Civil and Environmental Engineering, The George Washington University, Washington, DC 20052, USA*

*To whom correspondence should be addressed. E-mail: maohk@hpstar.ac.cn, or chenbin@hpstar.ac.cn

[#] F.K, Y.C and K.Y contributed equally to this work

www.pnas.org/cgi/doi/10.1073/pnas.1820890116

I. Materials and Methods

Sample preparation and electrical measurements in diamond anvil cells. Trilayer graphene flakes were mechanically exfoliated from bulk graphite on Si/SiO_2 surface. The layer number was determined with high-resolution microscopy and Raman spectra measurements. After the identification of thickness, trilayer graphene was then transferred onto diamond surface using a polydimethylsiloxane (PDMS) stamping technique as described in the previous report (1). During the transfer process, high-resolution microscopy and Raman spectra measurements were adopted to confirm that sample was not left on the Si substrate and PDMS, *i.e.*, to make sure that the trilayer sample has been transferred onto the diamond surface without damage. Ti/Au film electrodes on diamond surface were then prepared using photo-lithography and electron beam deposition techniques. Platinum foil (2 μm in thickness) electrodes were connected to the Ti/Au film at the edge of insulating chamber to avoid the breaking of electrodes under compression. To insulate probing electrodes from the metallic gasket, a mixture of cubic boron nitride and epoxy was compressed into the indentation area of gasket. Electrical measurements were conducted with a PPMS-9 with temperature range of 2-300 K. Four samples with different pressure medium, Daphne 7373 and argon to create a quasi-static pressure conditions to protect the ultrathin samples and film electrodes from damage during compression, were tested. All the results are good reproducible except for slight discrepancy in the transition pressures.

Absorption measurements. High-pressure IR absorption measurements were

conducted using type-IIa diamonds with 300 μm culet in diameter at Beamline 1.4.3 of Advanced Light Source (ALS), Lawrence Berkeley National Laboratory (LBL) and Infrared Lab of National Synchrotron Light Source II (NSLS-II) at Brookhaven National Laboratory (BNL). Infrared spectra were performed on a Fourier transform infrared spectrometer coupled to a microscope with a mid-band MCT detector. Transmittance spectra were measured for photon energy of 0.2-1.0 eV. Ruby spheres were used for calibrating pressure for all experiments. Three samples with different pressure medium, KBr, Daphne 7373 and argon were prepared for the measurements. Visible-ultraviolet absorption measurements were conducted on a customized visible-ultraviolet microscope system with the photon energy of 1.4-4.9 eV. For better comparison with electrical measurements, KBr, Daphne 7373 or Argon were used as pressure media, respectively. We obtained the transmittance data of sample from two measurements, one being the transmission through the sample area and the other through pressure medium area beside the sample. With these two measurements, the background from diamond and pressure medium can be subtracted. The electrical, IR and UV-Vis absorption measurements are done independently in different trilayer graphene under pressure.

Raman characterization. Raman spectra were collected with Renishaw InVia spectrometer. The identification of layer number and stacking order of trilayer graphene were done using the 532 nm laser as the incident light and 50x Leica optical microscope.

II. Identification of trilayer graphene by Raman measurements.

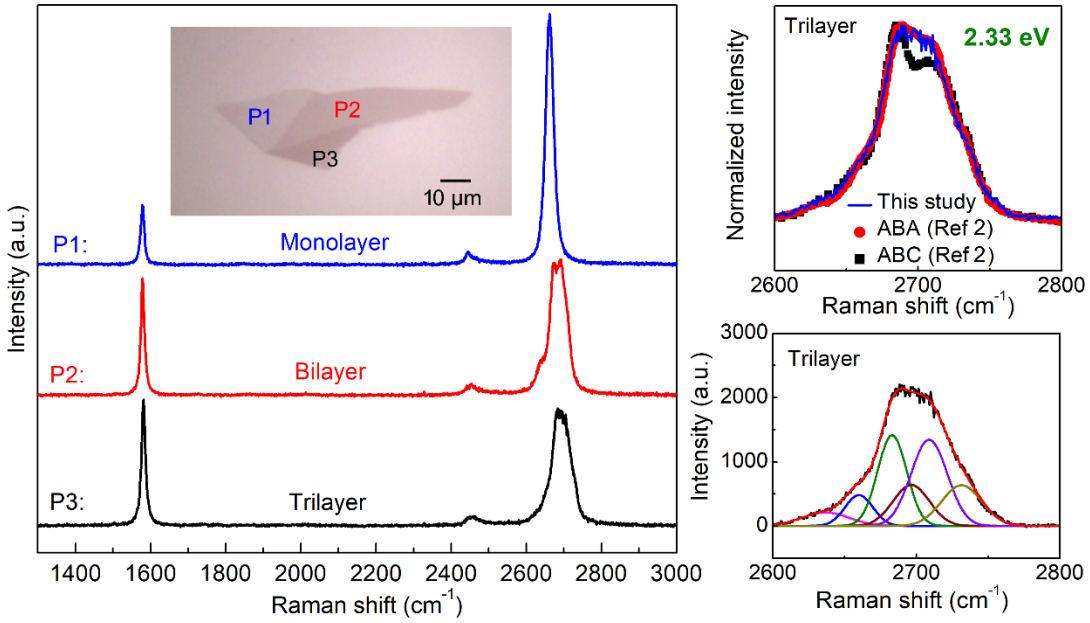

Fig. S1. Raman spectra of mono-, bi- and tri-layer graphene on Si/SiO_2 substrate [Left]. Trilayer samples were identified/verified with optical microscopy and Raman spectroscopy before and after transferring to diamond surface for measurements. The trilayer flake is of high quality without D-band. The Raman characterization indicates that trilayer graphene in our measurement has a Bernal (ABA stacking order) structure (2,3).

III. Contact tests and fitting of the R-T curves of trilayer graphene.

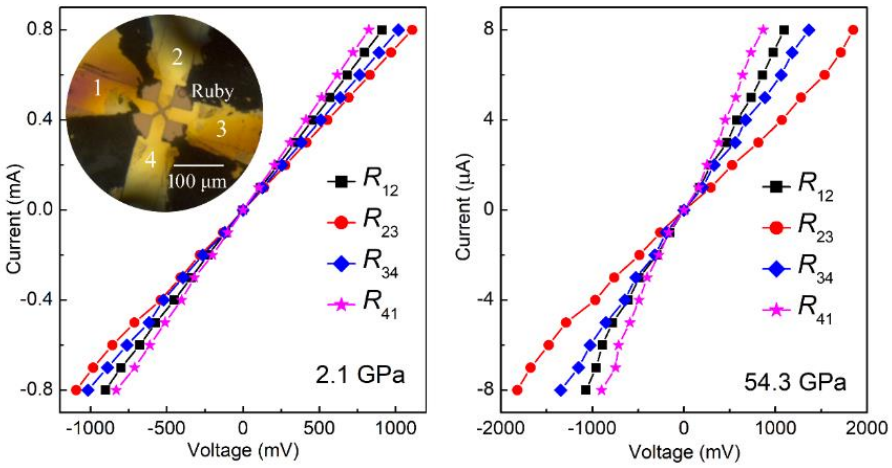

Fig. S2. Quality and reliability tests for the contacts between trilayer graphene, Ti/Au film electrodes under pressure. The *I*-*V* curves of adjacent channels show good linear behaviors, indicating the ohmic contact. The two-probe resistance of trilayer graphene is about 1.1 kΩ at 2.1 GPa and 140.5 kΩ at 54.3 GPa, respectively. The inset shows the optical microscopy image of sample and Ti/Au film electrodes under compression.

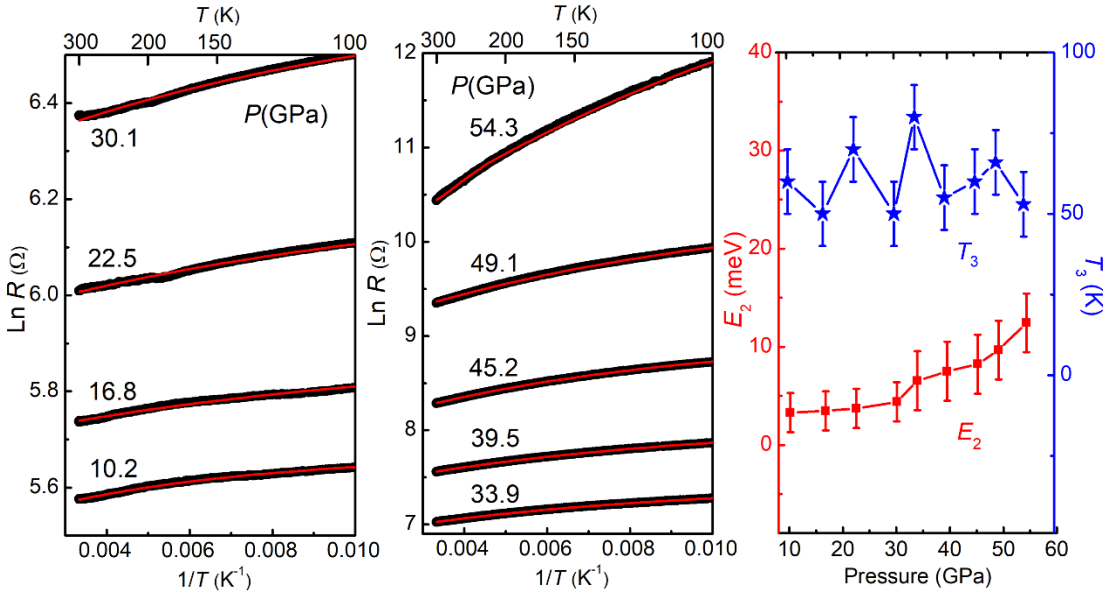

Fig. S3. Zoom in of the R-T curves of trilayer graphene at high temperature (Left) and the fitted E_2 and T_3 (Right) with Eq [1].

IV. UV-VIS absorption of trilayer graphene in diamond anvil cell.

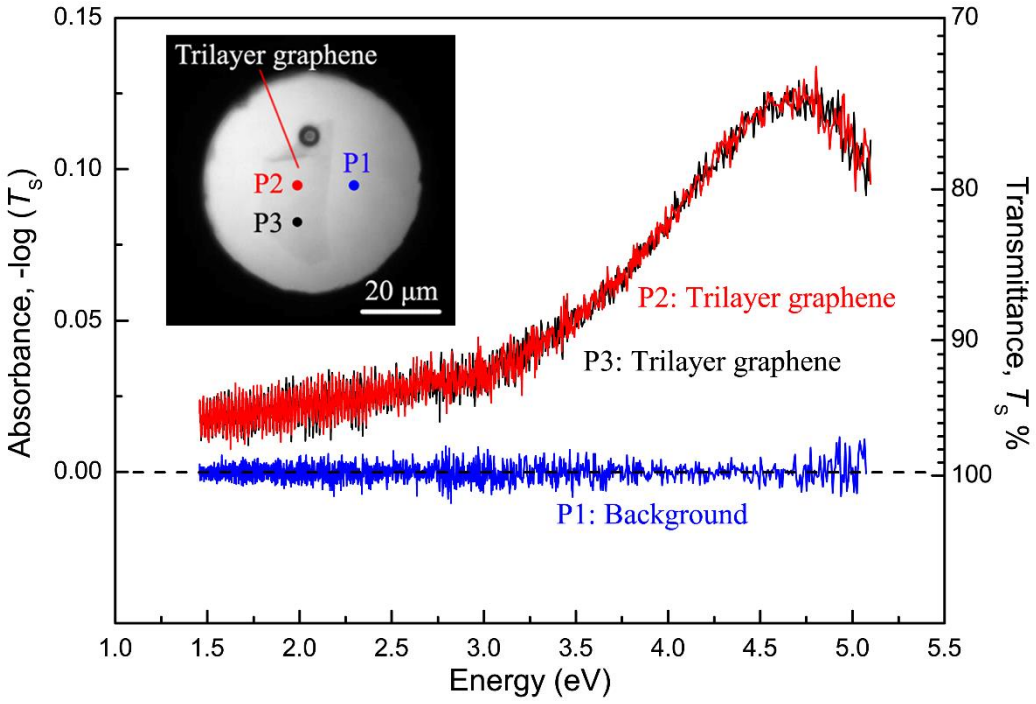

Fig. S4. UV-Vis absorbance patterns of trilayer graphene in diamond anvil cell at ambient conditions. The blue, black and red curves represent the background absorbance at P1 position, absorptance of trilayer graphene sample at P2 and P3 positions with background extracted, respectively. The spot size of incident light is about 10 μm in diameter. The inset shows the sample in diamonds anvil cell at ambient pressure illuminated with white transmitted light. A pronounced and asymmetric peak arising from the excitonic resonance at photon energy of ~4.64 eV is observed, similar to previously reported results on mono- and few-layer graphene (4,5). The light transmittance at photon energy of 1.5 eV is about 95.5%.

V. Synchrotron infrared absorption spectra of trilayer graphene.

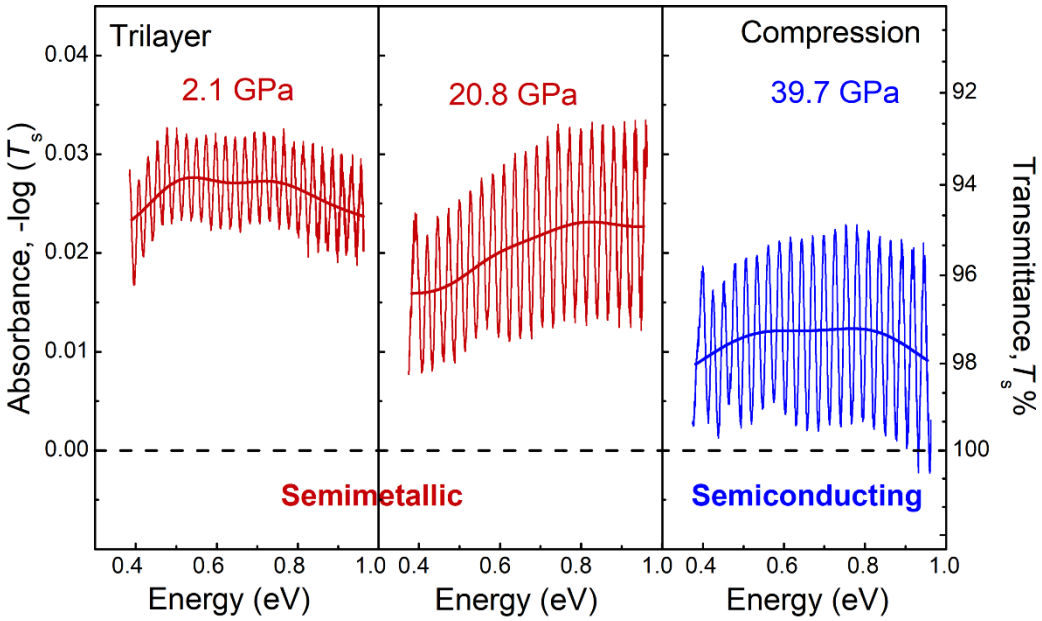

Fig. S5. Synchrotron infrared absorption spectroscopy of trilayer graphene under compression. The interference fringes in the curves are due to the high transparency of the ultrathin samples. The solid lines are the experimental data after subtracting the fringes with the Fourier transform Filter. Significant increase of transmittance is observed in trilayer graphene under compression.

VI. Determination of structural changes of trilayer graphene under compression.

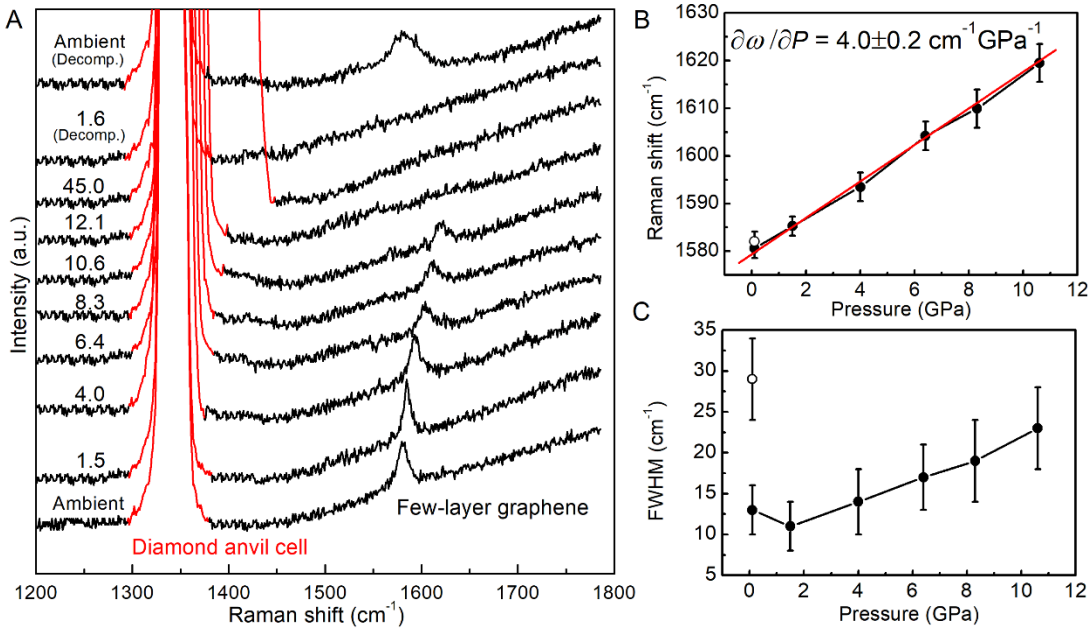

Fig. S6. (*A*) The Raman spectra of trilayer graphene under pressure. The G-band loses its intensity above 12.1 GPa, and reappears after quenching to ambient pressure, indicating the reversible transition. The D band of trilayer graphene (~1345 cm^{-1}, usually connected with the defects) is coupled with the Raman signal of diamond anvil cell (red peaks), which usually shifts to high frequency with pressure. (*B*) and (*C*) The Raman shift and width (full width at half maximum: FWHM) of G-band with pressure.

VII. Determination of bandgap of trilayer graphene.

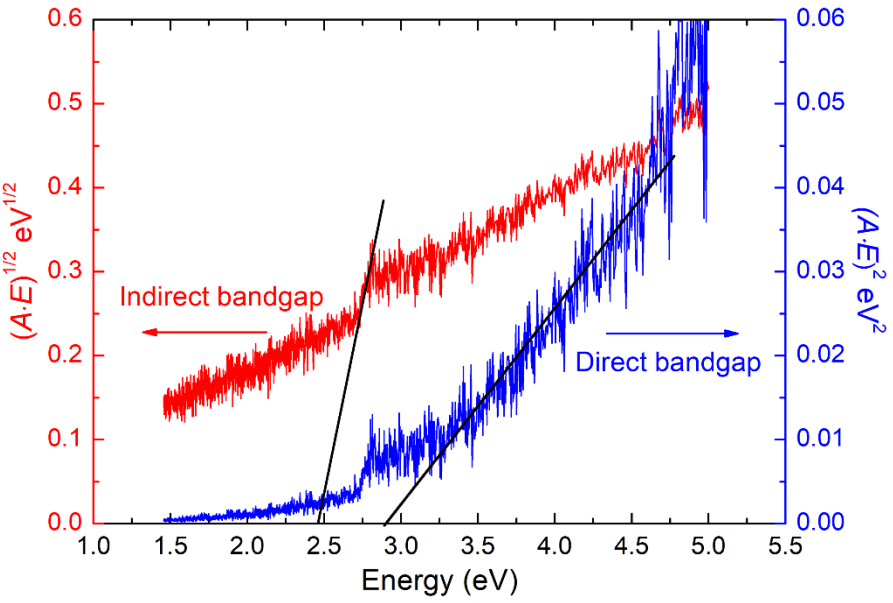

Fig. S7. Determination of bandgap of compressed trilayer graphene. The sharpness of the edge resembles that of an indirect gap. However, it is difficult to ascertain the gap nature due to the weak absorption signal of compressed trilayer graphene. We adopt the Tauc plot, i.e., $(A\cdot E)^{1/2}\sim E$ and $(A\cdot E)^{2}\sim E$, to analyze the data and obtain a bandgap by fitting the linear region (6). Usually, clear and dramatic drop can be observed in $(A\cdot E)^{2}\sim E$ curve for direct transition. The weak absorption edge of ~2.5 eV is so small in the $(A\cdot E)^{2}\sim E$ curve of compressed trilayer graphene, inconsistent with the character of direct transition. Hence, we assign it as an indirect absorption edge. By fitting the absorption edge in the $(A\cdot E)^{1/2}\sim E$ curve, an indirect bandgap of 2.5±0.3 eV is obtained. The pronounced and linear drop at 3.2~4.5 eV in the $(A\cdot E)^{2}\sim E$ curve resembles the character of direct transition. Hence, we fit this energy range and obtain a direct bandgap of 2.9±0.3 eV.

VIII. Nonuniformity of the semimetallic-semiconducting transition with pressure and its effect on activation energy and optical bandgap.

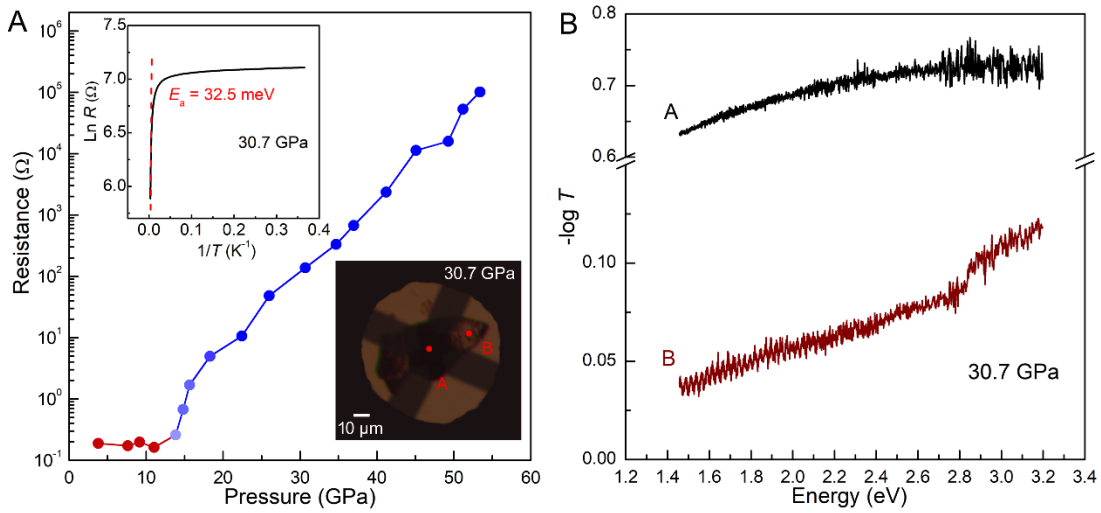

Fig. S8. The simultaneously measured electrical and absorption results of multilayer graphene (mechanically exfoliated from bulk graphite, 500 nm in thickness) to check the nonuniformity of simimetallic-semiconducting transition under pressure. (*A*) The pressure dependence of sheet resistance of multilayer graphene and the Arrhenius plots [ln *R* vs (1/*T*)] of the resistance-temperature curves at 30.7 GPa to fit the activation energy. An activation energy of 32.5 meV is obtained. The inset shows the optical microscope image of multilayer graphene with transmitted mode under white light. The non-uniform transparency of compressed multilayer graphene suggests the mixture state. (*B*) The absorption spectra of multilayer samples at position A (black area) and B (transparent area) shown in the inset of (*A*). A weak absorption edge at 2.5±0.3 eV is observed in the transparent area B, which is larger than that of the activation energy obtained by the electrical measurements.

1. Tongay S, *et al.* (2014) Tuning interlayer coupling in large-area heterostructure with CVD-grown MoS_2 and WS_2 monolayers. *Nano Lett.* 14: 3185-3190.

2. Cong C, *et al.* (2011) Raman characterization of ABA- and ABC-stacked trilayer graphene. *ACS Nano* 5: 8760-8768.

3. Lui C, *et al.* (2011) Imaging stacking order in few-layer graphene. *Nano Lett.* 11, 164-169.

4. Mak KF, Shan J, Heinz TF (2011) Seeing many-body effects in single- and few-layer graphene: observation of two-dimensional saddle-point exticons. *Phys. Rev. Lett.* 106: 046401.

5. Mak KF, Ju L, Wang F, Heinz TF (2012) Optical spectroscopy of graphene:from the far infraed to the ultraviolet. *Solid State Commun.* 152: 1341-1349.

6. Tauc J, Grigorovici R, Vancu A (1966) Optical Properties and ElectronicStructure of Amorphous Germanium. *Phys. Stat. Sol.* 15: 627-637.